A Comparative Study of Rainfall Retrievals Based on Specific Differential Phase Shifts at X- and S-Band Radar Frequencies

SERGEY Y. MATROSOV

Cooperative Institute for Research in Environmental Sciences, University of Colorado, and NOAA/Earth System Research Laboratory, Boulder, Colorado

ROBERT CIFELLI, PATRICK C. KENNEDY, STEVEN W. NESBITT, AND STEVEN A. RUTLEDGE

Department of Atmospheric Science, Colorado State University, Fort Collins, Colorado

V. N. BRINGI

Department of Electrical Engineering, Colorado State University, Fort Collins, Colorado

BROOKS E. MARTNER

Cooperative Institute for Research in Environmental Sciences, University of Colorado, and NOAA/Earth System Research Laboratory, Boulder, Colorado

ABSTRACT

A comparative study of the use of X- and S-band polarimetric radars for rainfall parameter retrievals is presented. The main advantage of X-band polarimetric measurements is the availability of reliable specific differential phase shift estimates, K_{DP}, for lighter rainfalls when phase measurements at the S band are too noisy to produce usable K_{DP}. Theoretical modeling with experimental raindrop size distributions indicates that due to some non-Rayleigh resonant effects, K_{DP} values at a 3.2-cm wavelength (X band) are on average a factor of 3.7 greater than at 11 cm (S band), which is a somewhat larger difference than simple frequency scaling predicts. The non-Rayleigh effects also cause X-band horizontal polarization reflectivity, Z_{eh}, and differential reflectivity, Z_{DR}, to be larger than those at the S band. The differences between X- and S-band reflectivities can exceed measurement uncertainties for Z_{eh} starting approximately at $Z_{eh} > 40$ dBZ, and for Z_{DR} when the mass-weighted drop diameter, D_m, exceeds about 2 mm. Simultaneous X- and S-band radar measurements of rainfall showed that consistent K_{DP} estimates exceeding about $0.1° $ km^{-1} began to be possible at reflectivities greater than ~26–30 dBZ while at the S band such estimates can generally be made if $Z_{eh} > $ ~35–39 dBZ. Experimental radar data taken in light-to-moderate stratiform rainfalls with rain rates R in an interval from 2.5 to 15 mm h^{-1} showed availability of the K_{DP}-based estimates of R for most of the data points at the X band while at the S band such estimates were available only for R greater than about 8–10 mm h^{-1}. After correcting X-band differential reflectivity measurements for differential attenuation, Z_{DR} measurements at both radar frequency bands were in good agreement with each other for $D_m < 2$ mm, which approximately corresponds to $Z_{DR} \approx 1.6$ dB. The Z_{DR}-based retrievals of characteristic raindrop sizes also agreed well with in situ disdrometer measurements.

1. Introduction

Polarimetric approaches for retrievals of rainfall parameters have been used with research radars for more

Corresponding author address: S. Y. Matrosov, NOAA/Earth System Research Laboratory, R/PSD2, 325 Broadway, Boulder, CO 80305.
E-mail: Sergey.Matrosov@noaa.gov

than 20 yr (Bringi and Chandrasekar 2001). These approaches were first developed and tested with longer-wavelength radars operating at S ($\lambda \sim 11$ cm) and C ($\lambda \sim 5$ cm) bands because these band frequencies are customarily used for quantitative precipitation estimations (QPE; e.g., Ryzhkov and Zrnic 1995; May et al. 1999; Brandes et al. 2001). Meteorological X-band ($\lambda \sim 3$ cm) radars have been traditionally limited in their applicability for QPE due to relatively high attenuation

(differential attenuation) rates of reflectivity, Z_{eh} (differential reflectivity, Z_{DR}), in rain. In the last few years or so, however, several polarimetric X-band radars have been introduced worldwide (e.g., Iwanami et al. 2001; Martner et al. 2001; Wurman 2001; Gosset and Cazenave 2003) for hydrometeorological applications.

The newly expressed interest in meteorological applications of X-band radars is motivated to a large degree by the introduction into practical use of special polarimetric procedures that have been developed to correct radar power measurements for effects of attenuation and differential attenuation (e.g., Bringi and Chandrasekar 2001). These correction procedures greatly mitigate signal attenuation issues and significantly extend the usable range of X-band radar QPE measurements (e.g., Matrosov et al. 2002, 2005; Anagnostou et al. 2004). Total signal loss, however, can occur at longer ranges in heavy rain, thus making X-band radars effective for QPE at generally shorter ranges (~50 km or so) compared to S-band radars (~150 km or so) that have been thus far a standard in the meteorological radar polarimetry.

Aside from this important range limitation, X-band polarimetry can offer some important practical advantages over longer-wavelength radar polarimetry at shorter ranges and lighter rainfall rates. One advantage is a significantly stronger differential phase shift on propagation, which is proportional to the radar frequency (for Rayleigh scattering). This allows the use of specific differential phase shift (K_{DP})-based rainfall estimators for lighter rainfall rates when measured with X-band radars than when measured with longer-wavelength radars. These signal phase–based estimators have important advantages over the power-based estimators (Zrnic and Ryzhkov 1996) due to their relatively weaker dependence on details of raindrop size distributions (DSDs) compared to the reflectivity-based estimators, their independence of the absolute radar calibration, the effects of partial signal attenuation and beam blockage, and also their lesser susceptibility to hail presence.

Other important advantages of X-band radars are that they are smaller, less expensive, require less energy for the same sensitivity, and are more easily transported compared to their longer-wavelength counterparts. These traits make X-band radars a convenient tool for QPE where high-resolution rainfall measurements are needed in a limited area such as a relatively small watershed or for specialized studies like those in urban hydrology. These radars are also useful in filling the gaps in the Weather Surveillance Radar-1988 Doppler (WSR-88D) network coverage over crucial basins in flood-prone areas like those on the northern California coast (Matrosov et al. 2005).

This paper presents a study of the comparative use of S- and X-band polarimetric radars for measurements of light-to-moderate rains that contribute a significant fraction of annual accumulations in many parts of the world. This study is mostly focused on assessments of extending the applicability of the specific differential phase shift (K_{DP}) approach for QPE of lighter rains when switching from S- to X-band frequencies because it is with this approach that the differences between these two bands are the most profound, and X-band advantages are more obvious. The question of differences in differential reflectivity (Z_{DR}) values in rainfall measurements at the S and X bands is also addressed.

2. Theoretical considerations

For Rayleigh scattering, reflectivity and differential reflectivity do not depend on the radar wavelength (except for minor variations due to the wavelength dependence of the complex refractive index of water), and K_{DP} values are proportional to the reciprocal of the wavelength. Although raindrops usually do not exceed about 6 mm in size (as expressed in diameters of the equal-volume sphere) and they are still relatively small compared to the X-band wavelengths, there are already some non-Rayleigh effects that might be noticeable. To assess the magnitude of these effects, calculations were performed of the individual drop ratio of differential reflectivity (r_{ZDR}), the wavelength-scaled ratio of specific differential phase (r_{KDP}), and the wavelength-scaled ratio of the horizontal polarization backscatter cross sections (r_Z) as functions of the equal-volume spherical drop diameter (D) for 5°C temperature. The results are shown in Fig. 1. The coefficients r_{ZDR}, r_Z, and r_{KDP} are defined as

$$r_{ZDR} = [\sigma_{hx}(D)/\sigma_{vx}(D)][\sigma_{hs}(D)/\sigma_{vs}(D)]^{-1},$$

$$r_{KDP} = \{\lambda_x^2 Re[f_{hx}(D) - f_{vx}(D)]\}$$
$$\times \{\lambda_s^2 Re[f_{hs}(D) - f_{vs}(D)]\}^{-1}, \quad (1)$$

$$r_z = [\sigma_{hx}(D)/\sigma_{hs}(D)](\lambda_x/\lambda_s)^4, \quad (2)$$

where σ_{hx}, σ_{vx}, σ_{hs}, σ_{vs} are the horizontal (h) and vertical (v) polarization backscatter cross sections at the common S-band ($\lambda_s = 11$ cm) and X-band ($\lambda_x = 3.2$ cm) wavelengths, and f_{hx}, f_{vx}, f_{hs}, f_{vs} are the forward-scattering amplitudes at these polarizations and wavelengths. As is usual in radar polarimetric modeling, the raindrops were modeled as oblate spheroids. The vertical orientation of drop symmetry axes and the low-elevation incidence (1°) were assumed.
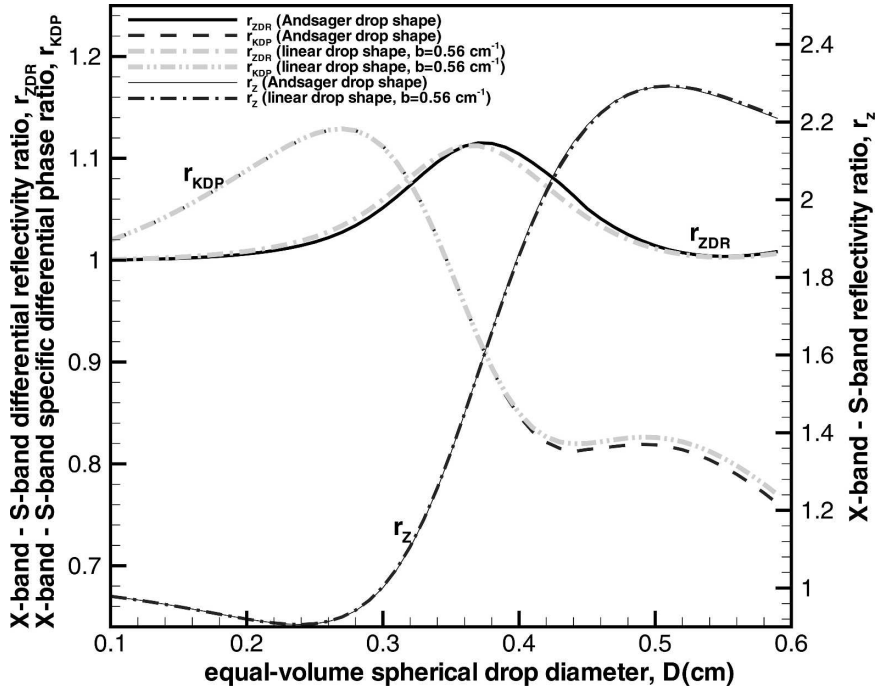
FIG. 1. Here r_{ZDR}, r_{KDP}, and r_Z as functions of raindrop size.

Calculations of r_{ZDR}, r_{KDP}, and r_Z were performed using the T-matrix approach (Barber and Yeah 1975) for the aspect ratio $(r) -$ equal-volume drop diameter (D) dependence given by a broken linear relation:

$$r = 1 (D \le 0.05 \text{ cm}),$$

$$r = (1.0 + 0.05b) - bD (D > 0.05 \text{ cm}), \quad (3)$$

and the combination of the aspect ratios suggested by Andsager et al. (1999) (for $D < 0.44$ cm) and the linear relation that approximates the equilibrium drop shape (for very large drops with $D \ge 0.44$ cm):

$$r = 1.012 - 0.144D - 1.03D^2 (D < 0.44 \text{ cm})$$

$$r = 1.02 - 0.62D (D \ge 0.44 \text{ cm}). \quad (4)$$

The shape factor b in (3) was assumed to be 0.56 cm^{-1}, which is close to the mean value of this parameter found using polarimetric retrievals (Gorgucci et al. 2000; Matrosov et al. 2005). This value of b is smaller than $b = 0.62$ cm^{-1}, which was used for a long time in the polarimetric community for calculations utilizing the linear model. It reflects the fact that raindrops are on average less oblate than the equilibrium drop shape predicts. Note also that (3) assumes the spherical shape for raindrops with $D < 0.05$ cm, unlike the simple linear line given by the formula $r = 1 - bD$, which is also sometimes used for drop shape modeling.

If scattering were strictly of the Rayleigh type, then $r_{ZDR} = r_{KDP} = r_Z = 1$. The deviations from the Rayleigh-type scattering at the X band results in a slightly greater increase of X-band K_{DP} values (compared to the S band) for drops with $D < 0.35$ cm than if predicted by simply scaling wavelengths. For larger drops, r_{KDP} decreases with size and then oscillates. The coefficient r_{ZDR} shows a broad maximum near drop sizes between 0.35 and 0.4 cm, and the individual drop Z_{DR} values at the X band remain greater than those at the S band for practically all raindrops sizes. Backscatter cross sections of raindrops at the X band exhibit the Rayleigh-like behavior (i.e., $r_Z \approx 1$) for $D < 0.3$ cm, after which r_Z rapidly increases with drop size reaching a maximum value of about 2.3 ($\sim$3.6 dB) at $D \approx 0.5$ cm.

It can be seen from Fig. 1 that the choice of the drop aspect ratio model does not influence the results in any significant way. Allowing a canting angle spread σ_α around the mean vertical orientation of drop axes decreases individual specific phase shifts by a factor of $\exp(-2\sigma_\alpha^2)$ (Oguchi 1983), and does not noticeably alter the results presented in Fig. 1 for common values of the canting angle spread ($\sigma_\alpha \sim 5°$–$10°$).

Deviations from the Rayleigh-type behavior of the raindrop forward-scattering amplitudes and backscatter cross sections at the X band result in the fact that K_{DP} values at X and S bands for actual rainfalls are not exactly scaled by wavelength, and Z_{DR} and the horizontal polarization reflectivities (Z_{eh}) values at these

bands are not equal. To illustrate this fact, calculations of K_{DP}, Z_{DR}, and reflectivity ratios at the X and S bands were performed using experimental DSDs that were recorded by an impact Joss–Waldvogel disdrometer (JWD) deployed at the Boulder Atmospheric Observatory (BAO) during May–July of 2004. Overall, about 5000 one-minute DSDs were recorded during this period. The dead-time correction (Sheppard and Joe 1994) for the JWD data and the site altitude (about 1600 m above sea level) correction were taken into account when interpreting measured DSD data.

Figures 2a,b show results of these calculations for the ratios $K_{DP}(3.2 \text{ cm})/K_{DP}(11 \text{ cm})$ and the logarithmic differences $\Delta Z_{DR} = Z_{DR}(3.2 \text{ cm}) - Z_{DR}(11 \text{ cm})$ for both assumptions of raindrop shapes. Since very light rains exhibit very weak polarization patterns, only DSDs that resulted in rainfall rates $R > 2.5 \text{ mm h}^{-1}$ were used for this modeling. The results in this figure show that, though appreciable data scatter exists, X-band K_{DP} is on average a factor of about 3.7 greater than S-band K_{DP}, while simple Rayleigh scaling for this particular choice of the wavelengths predicts a factor of 3.44. There is no significant dependence of the K_{DP} ratio on rainfall rate or on the drop aspect ratio–size relation, which, in part, can be explained by the broadness of the r_{KDP} maximum at around $D \approx 0.27 \text{ cm}$.

It can be expected that a higher differential phase accumulation rate at the X band would provide appreciable and thus usable K_{DP} values in rains when S-band phase measurements are too noisy to provide sensible K_{DP} estimates. In heavier rains when both S- and X-band K_{DP} values are available, smaller integration paths can potentially be used at the X band to accumulate the same phase difference, thus providing a better spatial resolution for K_{DP}-based rainfall estimators.

It can also be seen in Fig. 2b that X-band differential reflectivity values are larger than those at the S band. The differences ΔZ_{DR} are, however, relatively small for the mean mass-weighted raindrop diameters $D_m < 0.2$ cm, and they rarely exceed 0.2 dB, which is of the order of a typical uncertainty of Z_{DR} measurements. There is some tendency for ΔZ_{DR} to increase with D_m, and for $D_m > 0.2$ cm, it can result in X-band Z_{DR} being several tenths of decibels higher compared to the S band. This difference is large enough to take into account when using differential reflectivity data. However, ΔZ_{DR} values obtained in this study are somewhat smaller than those presented earlier by Holt (1984), whose calculations using exponential model DSDs resulted in X-band Z_{DR} being more than 0.5 dB higher than S-band Z_{DR} for $D_m > 0.15$ cm.

Figure 2c presents the differences ΔZ_{eh} of horizontal polarization reflectivities at X and S bands. For the
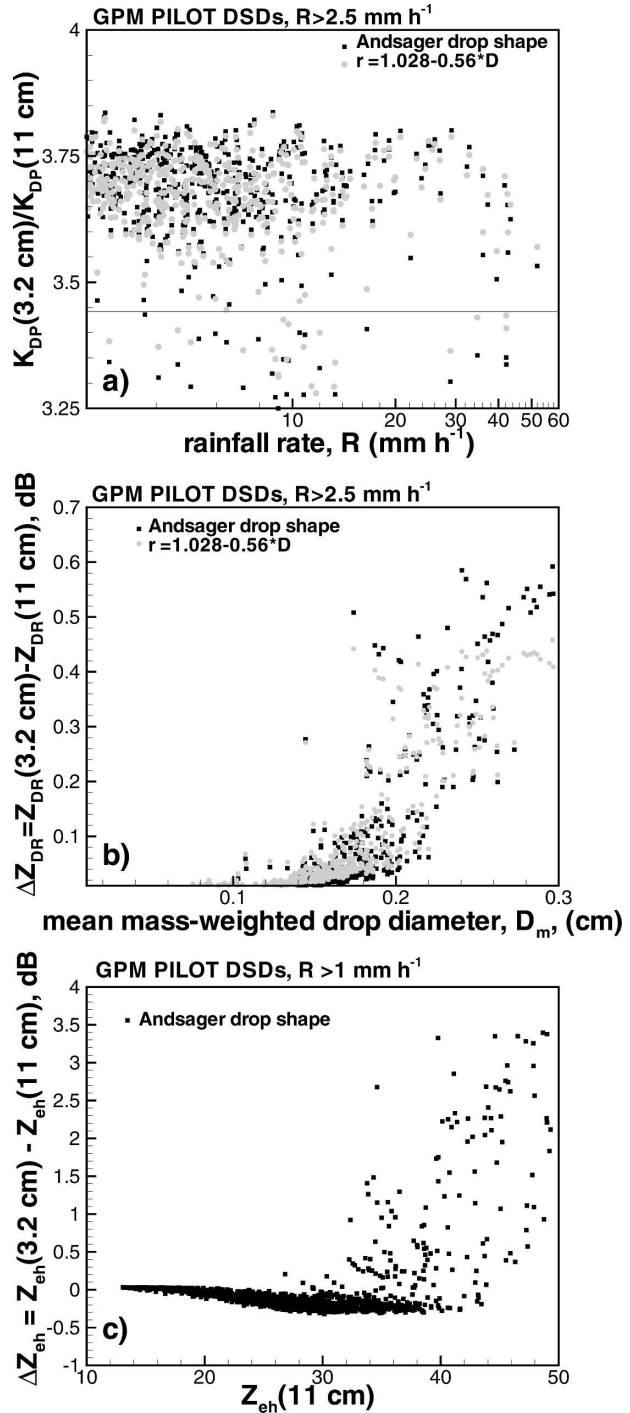

FIG. 2. Ratios of (a) K_{DP}, (b) Z_{DR}, and (c) Z_h differences at X and S bands for experimental DSDs.

great majority of the data presented in this figure (95% of the data points with $R > 1 \text{ mm h}^{-1}$), $|\Delta Z_{eh}| < 0.5$ dB, which is less than a typical uncertainty of reflectivity measurements. However, for some DSDs with larger drop sizes, the X-band reflectivities can exceed those at

the S band by more than 2 or 3 dB. For example, due to non-Rayleigh effects, for reflectivities larger than about 40 dBZ, values of Z_{eh} at the X band can be higher than those at the S band by more than 2 dB, which should be included in accounting for these effects. There is no significant dependence on the drop shape model for the ΔZ_{eh}–Z_{eh} correspondence, so the data in Fig. 2c are shown only for the Andsager drop shape in (4).

3. X- and S-band K_{DP} in light-to-moderate rains

During a 2-month period (16 May 2004–15 July 2004), the National Oceanic and Atmospheric Administration (NOAA) Earth System Research Laboratory's (ESRL's) X-band polarimetric radar ($\lambda_x = 3.2$ cm; Martner et al. 2001; Matrosov 2004), and the Colorado State University–University of Chicago Illinois State Water Survey (CSU–CHILL) radar ($\lambda_s = 11$ cm) (Brunkow et al. 2000) were simultaneously observing rainfall in northeastern Colorado as part of the Global Precipitation Mission (GPM) Ground Validation (GV) pilot study. Although the radars were not collocated, the CSU–CHILL radar was covering the NOAA/ESRL X-band radar scan area, so both X- and S-band radar polarimetric data were available in a sector (0–39-km radius) between 60° and 180° azimuthal directions centered at 40.1°N, 105°W. Two ground sites equipped with high-resolution (0.01 in.) tipping-bucket rain gauges and disdrometers were available for verification of radar retrievals. One of these sites was located at BAO (6.5 km from the NOAA radar and 54.5 km from CSU–CHILL) and the other at the University of Colorado's Platteville (PLT) observatory (27.8 km from the NOAA/ESRL radar and 30.4 km from CSU–CHILL).

Since the beams of both radars were not aligned and not parallel over any of the resolution points, it is ambiguous to quantitatively compare S- and X-band K_{DP} values that are not directly measured but are rather calculated as range derivatives (along the beam) of directly measured differential phase Φ_{DP}. Despite this drawback, the GPM GV dataset is useful in the sense that it provides measurements of the same rainfall with both X- and S-band polarimetric radars. Thus, it is instructive to analyze the situations when acceptable X-band K_{DP} data exist while S-band K_{DP} data are mostly unusable.

An example of the lowest-elevation (elev = 0.5°) CSU–CHILL horizontal polarization reflectivity field taken in the common radar scanning area is shown in Fig. 3a. Figure 3b shows a corresponding field of S-band K_{DP} values calculated from the differential phase measurements. It is apparent from Fig. 3 that valid S-band K_{DP} information does not become available (exceeds
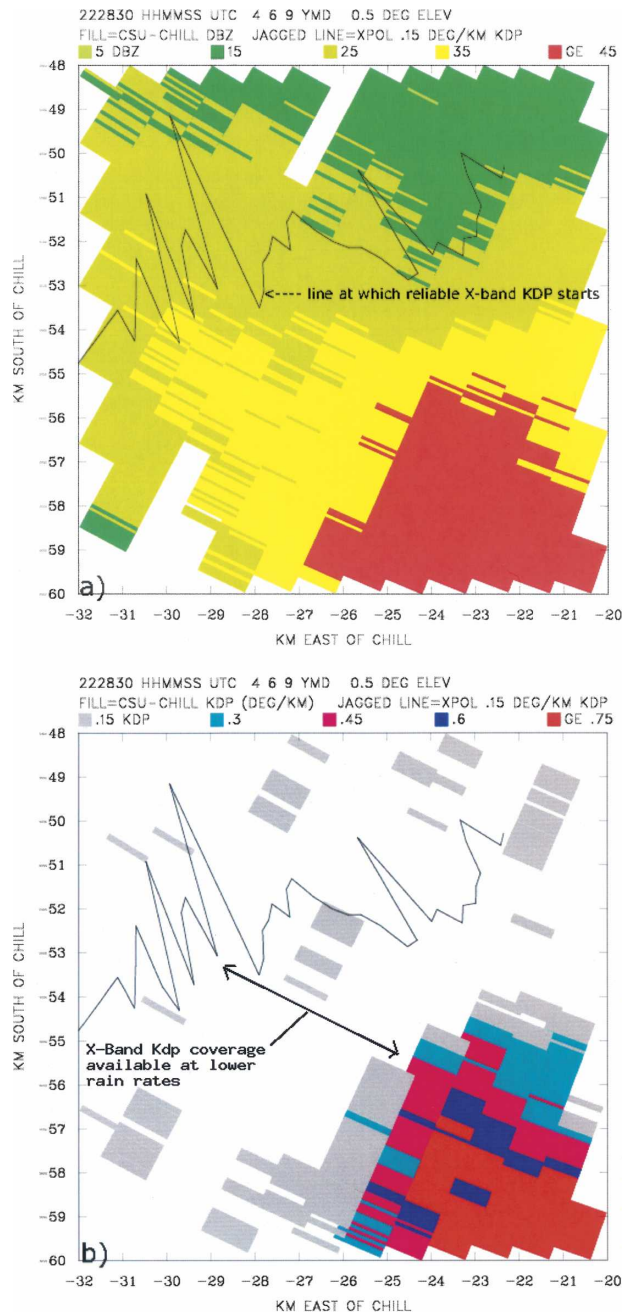

FIG. 3. CSU–CHILL PPI scan at 2228 UTC on 9 Jun 2004: (a) horizontal polarization reflectivity and (b) K_{DP}.

noise level) until reflectivity levels reach about ∼35–40 dBZ. The overlaid jagged line in Fig. 3 indicates the point along each radial of the NOAA/ESRL radar data (at elev = 1.8° to approximately match the altitude of X- and S-band data) at which X-band K_{DP} first reaches 0.1° km^{-1} in at least five contiguous 150-m-range gates. The X-band K_{DP} data began to become reliably available at reflectivity levels larger than ∼26–30 dBZ.

There is a relatively large area where meaningful S-band K_{DP} values are unavailable while X-band K_{DP} data are usable and can provide valuable retrieval information. The rainfall rates, R, in this area approximately correspond to an interval between 2 and 3 mm h^{-1} (at the lower end) and 8–12 mm h^{-1} (at the higher end). It is informative to analyze ground and radar data in more detail over the validation sites at BAO and PLT for rainfall rates in this interval. The situations of particular interest are stratiform rainfalls when the radar echoes cover relatively large areas. In stratiform rains, influences of the backscatter phase shift that might complicate the use of the X-band phase data are usually minor (Matrosov et al. 2005). For the purpose of this study, rain events with a clear brightband feature and reflectivities in the rain layer changing insignificantly in the vertical dimension (typically with gradients not exceeding 1–1.5 dB km^{-1}) are considered to be stratiform.

Light-to-moderate stratiform rains over BAO and PLT were observed by both radars on 17 and 21 June 2004. Data taken at 1.8° elevation angle were used for X-band data analysis to avoid contamination by ground clutter. The lowest elevation of CSU–CHILL (0.5°) was used for the data over BAO and 1.5° elevation data were used for the PLT analysis. The NOAA/ESRL radar beam was centered at about 900 m above the ground level (AGL) over PLT and at about 150 m over BAO. The center of the CSU–CHILL radar beam was positioned at about 700 m over PLT and at about 330 m over BAO. Note that the beamwidths of both radars are approximately the same (~0.9°). The melting level for the 21 June case was at about 1 km AGL over PLT, which resulted in contamination of the radar data by the ice phase, so PLT data for this case were not considered. On 17 June the melting level was higher than 1.5 km AGL, so there was no ice phase contamination of the radar data over either ground sites.

Figure 4 shows time series of horizontal polarization reflectivity data from both radars in a 150-m-resolution pixel over PLT and BAO for the stratiform rain events mentioned above. Since rainfall attenuation of radar power signals at the S band is negligible for such relatively modest rain rates, actual CSU–CHILL-measured reflectivities are shown in this figure. The X-band data in Fig. 4 represent reflectivities that were corrected for attenuation in rain along the propagation path between the radar and the resolution pixels above the ground sites using the NOAA/ESRL algorithm, which is described in detail by Matrosov et al. (2005). The rainfall rates, R, and Rayleigh reflectivities, calculated from DSDs recorded by JWD at the ground are also shown in this figure. The R values for the considered periods
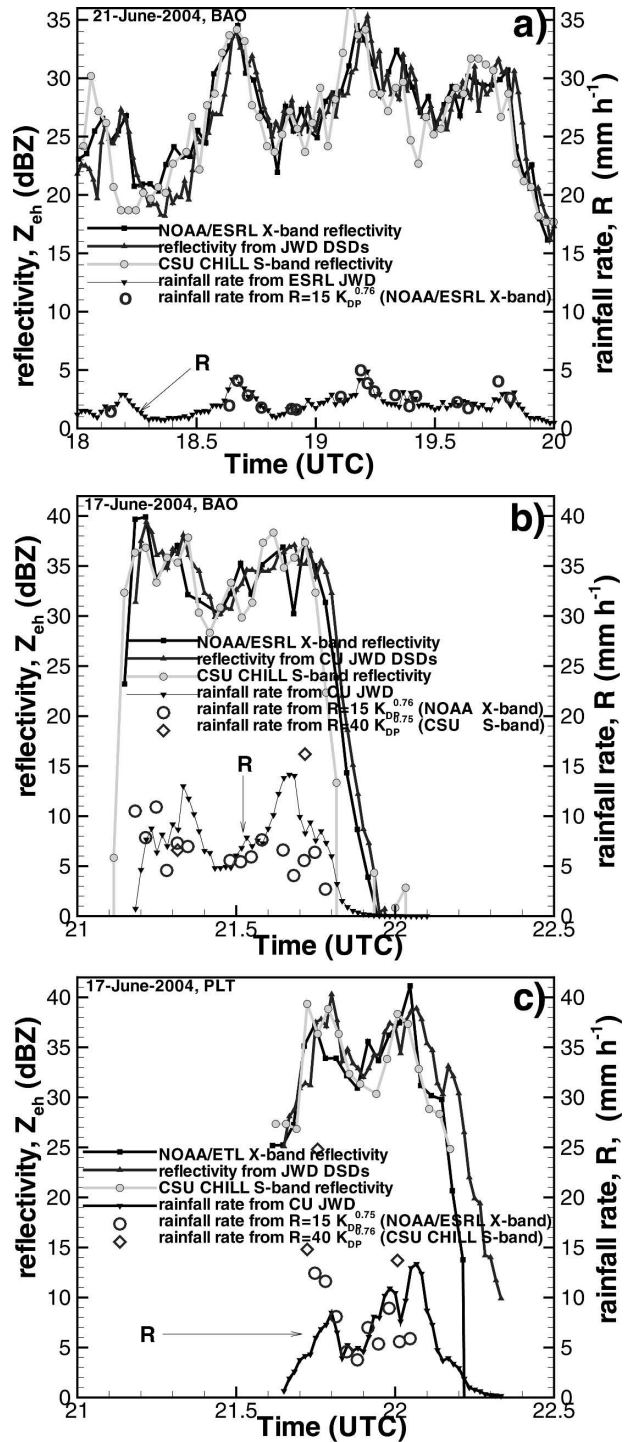

FIG. 4. Time series of reflectivities and rain rates for light-to-moderate rainfalls over BAO on (a) 21 June, (b) 17 June, and PLT on (c) 17 June.

are mostly between 2 and 10 mm h^{-1}, exceeding 10 mm h^{-1} only on occasion for a couple of very brief periods on 17 June. The rainfall rates from JWD could be considered reliable because total accumulations calculated

from JWD data were in good agreement with the collocated high-resolution (0.01 in.) tipping-bucket rain gauges, which were well calibrated.

It can be seen in Fig. 4 that there is generally good agreement between reflectivities from both radars and reflectivities calculated from JWD DSDs. The S-band reflectives during these cases do not exceed 40 dBZ, so according to the results presented in Fig. 2c, non-Rayleigh effects are not expected to be large enough to significantly influence the S–X-band radar reflectivity differences for most of the presented data except, probably, in the vicinity of the reflectivity maxima at around 21.2 (decimal) UTC on 17 June over BAO, and at around 21.8 and 22.1 UTC on 17 June over PLT, where S-band reflectivity is about 40 dBZ. In Fig. 4, the general locations of reflectivity maxima and minima observed by the radars closely match those obtained from in situ DSDs. Small time offsets between radar and ground data with the JWD-based reflectivities lagging behind the radar-observed reflectivities aloft are explained by the time required for raindrops to reach the ground. Given some possible vertical variability of the radar reflectivity field, the different altitudes of the centers of the radar beams, uncertainties of radar measurements and corrections, and also possible non-Rayleigh effects at the X band, there is good agreement between reflectivity data.

The NOAA/ESRL rain attenuation correction algorithm for the X-band reflectivity scales this correction with the radar-measured differential phase assuming a linear relation between K_{DP} and the specific attenuation coefficient A_h. A value of the correction coefficient $a_h = A_h/K_{DP} \approx 0.25$ dB deg^{-1} was found to satisfactorily describe attenuation effects in light-to-moderate rains (Matrosov et al. 2005) though one can expect a sizable increase in a_h in heavier rains (Carey et al. 2000) with larger median drop sizes ($D_o > 2.5$ mm, $Z_{DR} > 2.5$ dB).

For a subset of the GPM pilot X-band data, this algorithm was compared with the CSU self-consistent attenuation correction method with constraints (Bringi et al. 2001), which is based on the approach of Testud et al. (2000). This method was originally developed for the C band and then adjusted for X-band measurements. The comparisons of the NOAA/ESRL and CSU correction methods indicated fairly good agreement between two correction schemes, with the majority of the differences not exceeding about 1 dB, which is of the order of the uncertainty of reflectivity measurements. These comparison results and a general good correspondence between attenuation corrected X-band reflectivities and S-band observed reflectivities provide confidence in the applied attenuation correction scheme.

Figure 5 depicts K_{DP} over the ground sites calculated from the differential phase measurements at the X and S bands for the events shown in Fig. 4. The K_{DP} values were estimated along the respective radar beams using a 3.1-km sliding "window" interval, L, which approximately corresponds to 21 resolution range gates, Δr, for both radars. For K_{DP} calculations, the CSU algorithm smoothes the range profile of Φ_{DP} (Hubbert and Bringi 1995) while the NOAA/ESRL applies a least squares regression approach after having filtered out unreliable and questionable data points (Matrosov et al. 2002). This filtering excludes Φ_{DP} points that correspond to nonmeteorological echoes, spurious hardware responses and, to some extent, backscatter phase shifts.

To ensure compatibility of the CSU and NOAA/ESRL K_{DP} calculation approaches, both algorithms were compared for the same subset of the X-band dataset that was used for comparisons of attenuation corrections schemes. These comparisons indicated that the relative standard deviations between K_{DP} values from the two algorithms were typically within 30%, with a relative bias of less than 10%. These relative deviation values are comparable to the statistical uncertainty of K_{DP} data itself; thus, the agreement between these two different algorithms for the specific differential phase is considered to be quite satisfactory.

It can be seen in Fig. 5 that S-band K_{DP} data, except for a few data points on 17 June (e.g., times when Z_{eh} reached about 40 dBZ), are fluctuating erratically around zero and represent noise. The X-band K_{DP} data exhibit much less noisiness, and they are stably positive above 0.08°–0.1° km^{-1} for the time periods when rainfall rate exceeds about 2–3 mm h^{-1} (e.g., between 18.6 and 18.7, 19.15 and 19.25, 19.7 and 19.8 in decimal UTC on 21 June over BAO and most of the observation time for 17 June over both ground sites). These periods, as can be seen in Fig. 4, correspond to reflectivities greater than about 26–28 dBZ, which is in general accord with the results in Fig. 3.

In the ESRL X-band radar rainfall retrievals, a so-called K_{DP}-based method estimates rain rates for a particular resolution pixel from a K_{DP}–R relation when two conditions for specific differential phase and the corrected reflectivity are satisfied:

$$K_{DP} > K_{DP}^{(t)} = 0.09° \text{ km}^{-1} \qquad (5)$$

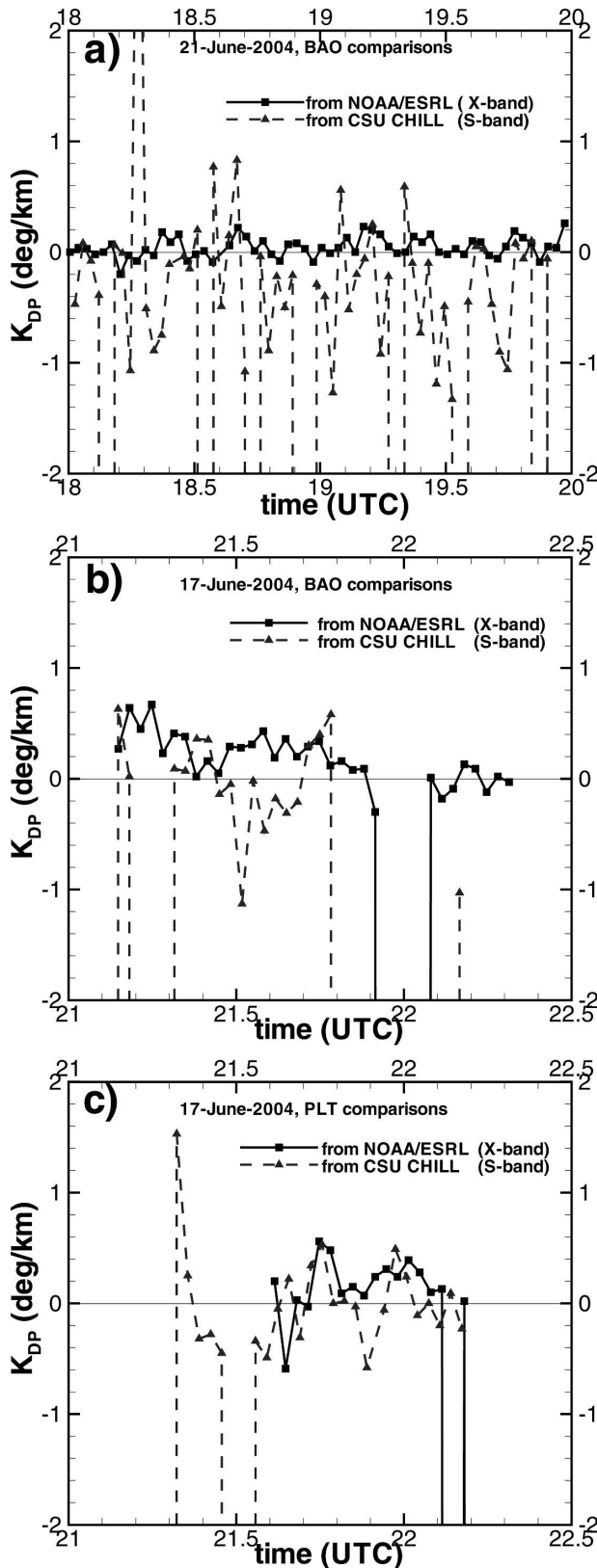and

$$Z_{eh} > Z_{eh}^{(t)} = 28 \text{ dB}Z. \qquad (6)$$

FIG. 5. Same as in Fig. 4, but for the X- and S-band K_{DP} estimates.

Otherwise, a mean Z_{eh}–R relation is used to calculate R from the radar reflectivity measurements corrected for attenuation. This particular value of $K_{DP}^{(t)}$ was chosen experimentally. It approximately corresponds to the theoretical standard deviation of specific differential phase shift estimates, SD(K_{DP}), using the least squares regression approach (Balakrishnan and Zrnic 1990),

$$\text{SD}(K_{DP}) = [\text{SD}(\Phi_{DP})/L][3L\Delta r/(L^2 - \Delta r^2)]^{0.5},$$

(7)

for a typical value of standard deviation of Φ_{DP} measurements [SD(Φ_{DP}) ~1.8° in steady rain] with a 150-m gate spacing (Δr) and a 5-km sliding "window" interval (L) that has often been used for previous NOAA/ESRL X-band rain measurements.

The K_{DP}-based method was found to provide a noticeable improvement over the traditional Z_{eh}–R approach (even when measured X-band reflectivities were corrected for attenuation in rain) in estimating total rainfall accumulations in the field experiments conducted in the coastal areas of northern California (Matrosov et al. 2005).

These thresholding values [i.e., $K_{DP}^{(t)} = 0.09°$ km^{-1} and $Z_{eh}^{(t)} = 28$ dBZ] were also used for the discussed GPM pilot experimental cases to retrieve rainfall rates. The corresponding retrievals of R derived from K_{DP} (when these retrievals are available based on thresholding) are shown in Fig. 4 superimposed on the estimates from JWD DSDs on the ground. Based on all DSDs collected during the entire GPM pilot field experiment, the mean X-band K_{DP}–R relation used here for the linear drop shape (3) with $b = 0.56$ cm^{-1} is

$$R = 15K_{DP}^{0.76}(\text{X band}).$$
(8)

It is rather close to the one found for the California coast data (i.e., $R = 14 K_{DP}^{0.8}$) for the same drop shape model. The GPM pilot DSD-based relation for the CSU CHILL wavelength is

$$R = 41K_{DP}^{0.75}(\text{S band}).$$
(9)

The same type of K_{DP} thresholding (5) was applied to the S-band data, however, reflectivity thresholding was applied in this case for $Z_{eh}^{(t)} = 38$ dBZ rather than 28 dBZ in order to reflect the fact that at the S band, consistent specific differential phase estimates start at higher reflectivities compared to the X band. It is not surprising, that no CSU–CHILL data points passed thresholding for the 21 June case over BAO (Fig. 4a), and only a couple of data points provided S-band K_{DP}-based rain-rate estimates for the 17 June case (Figs. 4b,c) when R values peaked above about 8–10 mm h^{-1}. In contrast to the S-band data, X-band K_{DP}-based

rain-rate estimates are available over both ground sites for most of the case on 17 June and for most of the time on 21 June when R values according to the ground JWD estimates were above ~2.5–3 mm h^{-1}. These X-band R retrievals generally agree with ground estimates; however, in a few instances, X-band data fail to capture some rain features recorded at the ground. One such example is the R maximum at around 21.65 decimal UTC on 17 June over BAO (Fig. 4b). This ground rain maximum also corresponds to the sudden drop in X-band reflectivity, suggesting that this could be a radar sampling issue.

It should be mentioned, however, that due to the general noisiness of phase measurements (especially at lower rainfall rates) and some dependence of K_{DP} values on the choice of the range interval used for deriving the phase derivative, K_{DP}-based approaches are better suited for retrievals of time (or space) integrated rainfall accumulations rather than for instantaneous values of R. Overall experimental results presented in this section show that the sensible K_{DP} data are generally available at the X band in light-to-moderate rains with R in the interval from about 2.5–3 to about 8–10 mm h^{-1} or so for which no reliable S-band K_{DP} data typically exist. For some practical cases, conditions (5)–(6) can be different. The increase of the thresholding values $K_{DP}^{(t)}$ [and/or those of $Z_{eh}^{(t)}$] would generally shift this rain-rate interval of availability of X-band K_{DP} data and lack of S-band K_{DP} data toward higher values of R. Such an increase could be warranted in some experimental cases when phase data are particularly noisy and/or rainfall is significantly nonuniform. The increase of the sliding window interval L used for calculating K_{DP} might help to somewhat extend the availability of sensible S-band K_{DP} estimates to lower rainfall rates at the expense of effective spatial resolution.

According to the ESRL JWD data from the GPM GV project, rainfall rates exceeded 10 mm h^{-1} only during 3% of total rainfall time of about 52 h for which $R > 0.1$ mm h^{-1}. The temporal fraction of rains with $R > 2.5$ mm h^{-1} was 20%, thus K_{DP}-based algorithms at the X band could be used about 6.5 times more often than at the S band. In terms of rain accumulation, rains with $R > 2.5$ mm h^{-1} produced about 67% of the total observed accumulation of 110 mm (for rains with $R > 0.1$ mm h^{-1}), while the accumulation fraction of rains with $R > 10$ mm h^{-1} was only 29%.

Although the above estimates of rainfall event occurrences for which X- and S-band K_{DP}-based algorithms can be used were obtained from the limited GPM GV dataset, they are in general agreement with a broader study of WSR-88D reflectivity statistics near the locations that are considered for the GPM continental

ground validation supersite (i.e., Wallops Island, Virginia; Ponka City, Oklahoma; Melbourne, Florida; and Huntsville, Alabama). This study indicates that, depending on the location, the occurrence of rainfall reflectivities greater than 38 dBZ is typically between about 3% and 6% and the occurrence of reflectivities greater than 28 dBZ is between 18% and 26%.

4. Comparisons of X- and S-band Z_{DR} measurements

Unlike K_{DP} data, which, under the Rayleigh assumption, are approximately scaled with frequency, differential reflectivity measurements at the X and S bands should be close to each other given that Z_{DR} data at the X band are corrected for differential attenuation and raindrop mass-weighted sizes do not significantly exceed 0.2 cm (see results in Fig. 2b). As for the attenuation correction schemes, the CSU differential attenuation correction method (Bringi et al. 2001) modified for X band was compared to the NOAA/ESRL method (Matrosov et al. 2005) for the same subset of the GPM-pilot X-band dataset. These comparisons indicated that there was practically no bias in corrected Z_{DR} using these methods for $Z_{DR} < 2$ dB. For larger Z_{DR} values, the NOAA/ESRL correction method produced slightly larger corrected values (by 0.1–0.2 dB on average) than the CSU method. These differences are smaller than typical errors of differential reflectivity measurements, thus it can be concluded that both differential attenuation correction algorithms were mutually consistent.

After the deployment of the NOAA/ESRL X-band radar and prior to the field work, X-band Z_{DR} measurements were calibrated in drizzle (approximately spherical drops) to ensure a proper calibration balance in the horizontal and vertical channels. The Z_{DR} calibrations of the CSU–CHILL radar are also regularly performed using carefully controlled observations of known hydrometeor types.

Figure 6 shows comparisons of X- and S-band Z_{DR} measurements over the ground sites for the same time periods as in Fig. 3. The X-band Z_{DR} data were corrected for differential attenuation using the NOAA/ESRL algorithm. Unlike K_{DP}, Z_{DR} is a point measurement; however, it is also somewhat noisy, and typical uncertainties of differential reflectivity measurements are of the order of 0.25 dB. To exclude relatively unreliable points, only data with $Z_{DR} > 0.25$ dB are plotted in Fig. 6. This removal of unreliable points mainly concerns the 21 June case over BAO (Fig. 6a), while most of the data points for the 17 June cases had Z_{DR} values from both radars greater than 0.25 dB (Figs. 6b,c).
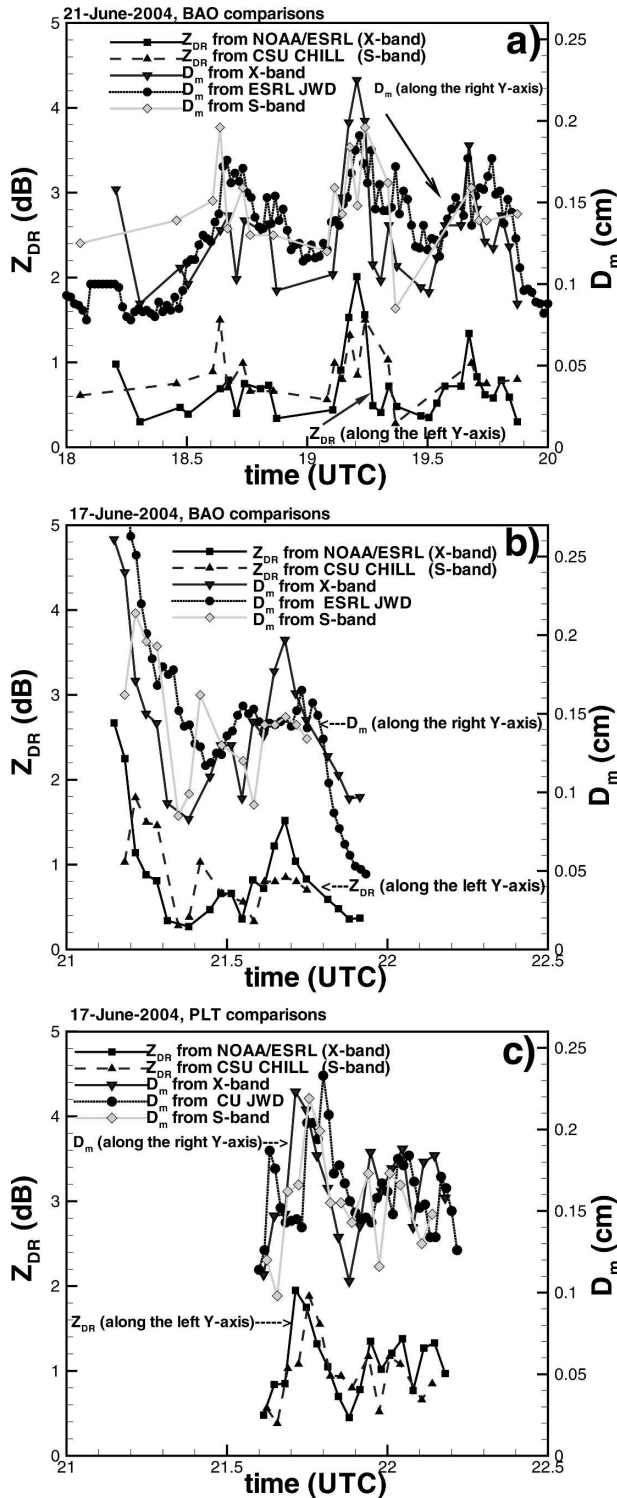
FIG. 6. Same as in Fig. 4, but for the X- and S-band Z_{DR} measurements and mass-weighted drop diameter D_m.

Given the 0.25-dB Z_{DR} measurement uncertainty, sampling volume differences, and possible 0.1–0.2-dB or so differences because of coupling of X-band polarimetric data due to the use of the simultaneous transmission–simultaneous receiving (STSR) scheme (Matrosov et al. 2002), S- and X-band Z_{DR} values track each other rather well. At some instances, however, X-band differential reflectivities were higher than those at the S band by 0.3–0.6 dB. Those instances include times (in decimal UTC) between 19.15 and 19.25 on 21 June, at around 21.2 and 21.7 on 17 June over BAO. Some of these times correspond to observations of larger drops ($D_m \geq 0.2$ cm) by the ground-based JWD (e.g., 21.2 UTC in Fig. 6b, 19.7 UTC in Fig. 6a), so the non-Rayleigh scattering effects shown in Fig. 2b might be, in part, responsible for these S–X-band differences.

The X-band estimator suggested for retrieving mass-weighted equal-volume sphere raindrop diameter (Matrosov et al. 2005)

$$D_m(\text{cm}) = 0.16 Z_{DR}^{0.49} \text{ (dB)} \text{ (for } Z_{DR} > 0.25 \text{ dB)}$$

(10)

was used here to retrieve D_m values, and the results of these retrievals are also shown in Fig. 6 along with the D_m estimates from JWD DSDs. The X-band estimator in (11) is very close to the one suggested by Bringi and Chandrasekar (2001) for the S band ($D_m = 0.1619 Z_{DR}^{0.485}$), so it was also used for calculating characteristic drop diameters from the CSU–CHILL data.

It can be seen in Fig. 6 that radar-retrieved drop sizes are in general agreement with the JWD data. Typical differences between D_m values from different sources (i.e., X-band data, S-band data, and JWD) are about 0.03 cm, which is what one would expect from about 0.25-dB uncertainty of the differential reflectivity measurement. One interesting fact is that X-band retrievals accurately capture larger drop sizes at around 21.2 UTC on 17 June over BAO (Fig. 6b). The corresponding D_m values are exceeding 0.2 cm and are likely to cause non-Rayleigh scattering at the X band.

Overall it can be concluded that differential reflectivity measurements at the X and S bands are comparable (for $Z_{DR} < 2$ dB), and the corresponding retrievals of characteristic raindrop sizes are in good agreement with JWD data. It indicates that X-band radars, as is true with their counterparts at the S band, can be used effectively for DSD parameter retrievals. While polarimetric S-band radars have been used for such retrievals for a long time (Bringi and Chandrasekar 2001), X-band radars are just beginning to be used for such purposes (Matrosov et al. 2005). Though it is expected that the quality of X-band Z_{DR}-based drop size

retrievals would gradually degrade with range, as uncertainties associated with differential attenuation corrections are likely to accumulate, it is encouraging to see especially good agreement between S- and X-band differential reflectivity measurements over PLT (Fig. 6c), which is located approximately at equal distances (~30 km) from both radars.

5. Conclusions

Theoretical calculations using the experimental raindrop size distributions and analyses of polarimetric measurements of light-to-moderate rainfalls were performed to assess a utility of X-band radar to complement longer wavelength radars that are traditionally used in radar meteorology. The dataset used in this study is one of the first such datasets that comprises the simultaneous X- and S-band polarimetric measurements of the same rainfall.

Besides physical size and cost issues, the main advantage of X-band polarimetric weather radars over longer wavelength radars is in the higher values of specific differential phase, K_{DP}, which is a valuable parameter for rainfall retrievals. The K_{DP} at 3.2 cm is larger than that at 11 cm by an average factor of 3.7, which is a little greater than simple Rayleigh wavelength scaling predicts. As a result of stronger differential phase signal, X-band K_{DP}-based rainfall estimates typically become meaningful at rainfall rates as low as 2.5–3 mm h^{-1}, which approximately corresponds to reflectivities of ~27–28 dBZ while such estimates at the S band begin to become meaningful at rain rates of 8–10 mm h^{-1} or $Z_{eh} \sim$ 37–38 dBZ. This allows use of X-band K_{DP}-based retrievals of rainfall rates and corresponding accumulations for light-to-moderate rains when such retrievals at the S band are not available. On average, for DSDs observed during the GPM GV project, these approximate conditions for applying K_{DP}-based retrievals at the X band were met 6.5 times more often compared to such conditions at the S band. More than twice as much of rainfall accumulation was observed when R was exceeding 2.5 mm h^{-1} than when R was greater than 10 mm h^{-1}. The aforementioned reflectivity and rain-rate limits of usefulness of X- and S-band specific differential phase shift–based rainfall estimates correspond to about 3–4-km range interval, L, that is used for K_{DP} calculations as a mean range derivative of Φ_{DP} data. Such values of L are typically used for K_{DP} calculations. Increasing L can potentially extend the use of K_{DP}-based retrievals toward somewhat lighter rainfall rates at both bands at the expense of more crude spatial resolution.

Although the X band has clear advantages over the S band for retrievals of light-to-moderate rainfall rates based on K_{DP}, there are no such advantages when using other polarimetric estimators (e.g., those that are based on Z_{eh} and Z_{DR}). The detailed comparable studies of K_{DP}-based rainfall algorithms with other polarimetric rainfall estimators for the GPM GV dataset are, however, beyond the scope of this study. It should also be mentioned that the independence of K_{DP} estimators of the radar absolute calibration and their generally lesser sensitivity to the DSD details (compared to the power-based estimators) make them rather attractive. It was also shown (Ryzhkov et al. 2005) that S-band estimators containing K_{DP} generally outperform power-based estimators (i.e., those based on Z_{eh} and Z_{DR}) for larger rainfall rates where specific differential phase signal at the S band is strong enough. This is for these traits among others; it was suggested to use K_{DP} (when it is reliably available) for rainfall rates retrievals with prospective polarimetrically upgraded S-band WSR-88D network radars (Ryzhkov et al. 2005).

One potential caveat for the use of K_{DP} at the X band is a possible contribution of the backscatter phase shift that can affect calculated K_{DP} values. The backscatter phase shift manifestations, however, are not very pronounced, especially in light-to-moderate rain (Matrosov et al. 2005) and they are mitigated by filtering the original differential phase (Φ_{DP}) measurements.

Modeling using experimental DSDs shows that the non-Rayleigh effects at the X band are generally small if reflectivities are less than about 40 dBZ. Thus, for such Z_{eh} values, the differences between X- and S-band reflectivities typically do not exceed measurement uncertainties. At reflectivities greater than 40 dBZ, non-Rayleigh effects can cause X-band reflectivities being higher than those at the S band by ~2–3 dB.

Differential reflectivity, Z_{DR}, at the X and S bands typically differ by no more than 0.25 dB for mean mass-weighted raindrop diameters, $D_m <$ 0.2 cm, and the corresponding differences can be neglected for most practical cases. For DSDs with $D_m >$ 0.2 cm, these differences can exceed ~0.3–0.4 dB, which is generally greater than typical uncertainties of Z_{DR} measurements. Simultaneous retrievals of D_m from Z_{DR} measurements at S and X bands indicated close results that were in good agreement with in situ estimates of drop sizes.

The general robustness of the X-band attenuation and differential attenuation correction algorithms is supported by the observed good agreement of the X-band-corrected Z_{eh} and Z_{DR} values with the corresponding values at the S band, which were essentially unattenuated for the considered light-to-moderate rainfall events. At longer ranges, however, X-band mea-

surements can be completely extinguished by cells of heavy rain. This limits the use of X-band radar rainfall retrievals to situations with light-to-moderate rains (and to shorter ranges if heavy rain cells are present) when the polarimetric schemes for correcting attenuation and differential attenuation effects can be used. Ideally, collocated matched-beam dual-wavelength (S and X bands) radar measurements of rainfall can combine the advantages of both bands, that is, the availability of stable polarimetric differential phase estimates for lighter rainfalls at X-band and longer-range coverage with negligible attenuation at the S band.

REFERENCES

Anagnostou, E. N., M. N. Anognostou, W. F. Krajewski, A. Kruger, and B. J. Miriovsky, 2004: High resolution rainfall estimation from X-band polarimetric radar measurements. *J. Hydrometeor., 5,* 110–128.

Andsager, K., K. V. Beard, and N. F. Laird, 1999: Laboratory measurements of axis ratios for large raindrops. *J. Atmos. Sci., 56,* 2673–2683.

Balakrishnan, N., and D. S. Zrnic, 1990: Estimation of rain and hail rates in mixed phase precipitation. *J. Atmos. Sci., 47,* 565–583.

Barber, P., and C. Yeh, 1975: Scattering of electromagnetic waves by arbitrarily shaped dielectric bodies. *Appl. Opt., 14,* 2864–2872.

Brandes, E. A., A. V. Ryzhkov, and D. S. Zrnic, 2001: An evaluation of radar rainfall estimates from specific differential phase. *J. Atmos. Oceanic Technol., 18,* 363–375.

Bringi, V. N., and V. Chandrasekar, 2001: *Polarimetric Doppler Weather Radar.* University Press, 636 pp.

——, T. D. Keenan, and V. Chandrasekar, 2001: Correcting C-band radar reflectivity and differential reflectivity data for rain attenuation: A self consistent method with constraints. *IEEE Trans. Geosci. Remote Sens., 39,* 1906–1915.

Brunkow, D., V. N. Bringi, P. C. Kennedy, S. A. Rutledge, V. Chandrasekar, E. A. Mueller, and R. K. Bowie, 2000: A description of the CSU-CHILL National radar facility. *J. Atmos. Oceanic Technol., 17,* 1596–1608.

Carey, L. D., S. A. Rutledge, D. A. Ahijevych, and T. D. Keenan, 2000: Correcting propagation effects in C-band polarimetric radar observations of tropical convection using differential propagation phase. *J. Appl. Meteor., 39,* 1405–1433.

Gorgucci, E., G. Scarchilli, V. Chandrasekar, and V. N. Bringi, 2000: Measurement of mean raindrop shape from polarimetric radar observations. *J. Atmos. Sci., 57,* 3406–3413.

Gosset, M., and F. Cazenave, 2003: Test of polarization based retrieval algorithms at X-band. Preprints, *31st Int. Conf. on Radar Meteorology,* Seattle, WA, Amer. Meteor. Soc., 805–808.

Holt, A. R., 1984: Some factors affecting the remote sensing of rain by polarization diversity radar in the 3- to 35-GHz frequency range. *Radio Sci., 19,* 1399–1412.

Hubbert, J., and V. N. Bringi, 1995: An iterative filtering technique for the analysis of copolar differential phase and dual-frequency radar measurements. *J. Atmos. Oceanic Technol., 12,* 643–648.

Iwanami, K., R. Misumi, M. Maki, T. Wakayama, K. Hata, and S. Watanabe, 2001: Development of a multiparameter radar system on mobile platform. Preprints, *30th Int. Conf. on Radar Meteorology,* Munich, Germany, Amer. Meteor. Soc., 104–106.

May, P. T., T. D. Keenan, D. S. Zrnic, L. D. Carey, and S. A. Rutledge, 1999: Polarimetric radar measurements of tropical rain at a 5-cm wavelength. *J. Appl. Meteor., 38,* 750–765.

Martner, B. E., K. A. Clark, S. Y. Matrosov, W. C. Campbell, and J. S. Gibson, 2001: NOAA/ETL's polarization-upgraded H-band "HYDRO" radar. Preprints, *30th Int. Conf. on Radar Meteorology,* Munich, Germany, Amer. Meteor. Soc., 101–103.

Matrosov, S. Y., 2004: Depolarization estimates from linear H and V measurements with weather radars operating in simultaneous transmission–simultaneous receiving mode. *J. Atmos. Oceanic Technol., 21,* 574–583.

——, K. A. Clark, B. E. Martner, and A. Tokay, 2002: X-band polarimetric radar measurements of rainfall. *J. Appl. Meteor., 41,* 941–952.

——, D. E. Kingsmill, B. E. Martner, and F. M. Ralph, 2005: The utility of X-band radar for quantitative estimates of rainfall parameters. *J. Hydrometeor., 6,* 248–262.

Oguchi, T., 1983: Electromagnetic wave propagation and scattering in rain and other hydrometeors. *Proc. IEEE, 71,* 1029–1078.

Ryzhkov, A. V., and D. S. Zrnic, 1995: Comparison of dual-polarization radar estimators of rain. *J. Atmos. Oceanic Technol., 12,* 249–256.

——, S. E. Giangrande, and T. J. Schuur, 2005: Rainfall estimation with a polarimetric prototype of WSR-88D. *J. Appl. Meteor., 44,* 502–515.

Sheppard, B. E., and P. I. Joe, 1994: Comparisons of raindrop size distribution measurements by a Joss–Waldvogel disdrometer, a PMS 2DG spectrometer, and a POSS Doppler radar. *J. Atmos. Oceanic Technol., 11,* 874–887.

Testud, J., E. L. Bouar, E. Obligis, and M. Ali Mehenni, 2000: The rain profiling algorithm applied to polarimetric weather radar. *J. Atmos. Oceanic Technol., 17,* 332–356.

Wurman, J., 2001: The DOW mobile multiple Doppler network. Preprints, *30th Int. Conf. on Radar Meteorology,* Munich, Germany, Amer. Meteor. Soc., 95–97.

Zrnic, D. S., and A. V. Ryzhkov, 1996: Advantages of rain measurements using specific differential phase. *J. Atmos. Oceanic Technol., 13,* 454–464.